



# Dust Condensation of SiC, SiO in Asymptotic Giant Branch Stellar Winds-SiC Spectrum

Ruiqing Wu<sup>1</sup>, Chunhua Zhu<sup>2</sup>, Guoliang Lü<sup>2</sup>, Shuming Yang<sup>3</sup>, Zhisen Meng<sup>3</sup>, Xiaojiao Zhang<sup>4</sup>, Xizhen Lu<sup>2</sup>, Jinlong Yu<sup>5</sup>,  
Wujin Chen<sup>6</sup>, and Mengqiu Long<sup>1</sup>

<sup>1</sup> School of Physics and Electronics, Central South University, Changsha 410083, China; [ruiqingwu163@163.com](mailto:ruiqingwu163@163.com), [mqlong@csu.edu.cn](mailto:mqlong@csu.edu.cn)

<sup>2</sup> School of Physical Science and Technology, Xinjiang University, Urumqi 830046, China

<sup>3</sup> School of Chemistry and Chemical Engineering, Guangxi University, Nanning 530004, China

<sup>4</sup> School of Microelectronics and Physics, Hunan University of Technology and Business, Changsha 410205, China

<sup>5</sup> College of Mechanical and Electronic Engineering, Tarim University, Alar 843300, China

<sup>6</sup> School of Medicine, Xinjiang Medical University, Urumqi 830011, China

Received 2024 February 12; revised 2024 March 16; accepted 2024 April 1; published 2024 May 2

## Abstract

We have chosen the Large Scale Atomic/Molecular Massively Parallel Simulator (LAMMPS) code to calculate the coalescence of silicon carbide (SiC), silicon oxide dust (SiO) in the AGB stellar wind. LAMMPS is a classical molecular dynamics simulation code. At the same time, we consider the effect of temperature on the evolution of molecular dynamics. We also calculated the temperature change of non-spherical SiC, SiO dust coalescence. The condensation temperature range of SiC dust in the AGB stellar wind is [300–500]k and [900–1100]k for SiO. Finally, the infrared spectrum of SiC was calculated using Gaussian 16 software. The 77SiC, 70Si<sub>3</sub>C<sub>3</sub>, and 121Si<sub>3</sub>C<sub>3</sub> models have clear characteristic peaks of infrared spectra responding at 5, 8.6, 11.3, 15, 19, and 37  $\mu\text{m}$ .

*Key words:* stars: AGB and post-AGB – infrared: ISM – (ISM:) dust – extinction

## 1. Introduction

During the asymptotic giant branch (AGB) phase, stars with an initial mass of up to  $8 M_{\odot}$  lose their outer stellar layers by means of a stellar outflow or wind. This creates an extended circumstellar envelope (CSE). The CSE is a rich astrochemical laboratory that has detected more than 100 molecules as well as newly formed dust species. The chemical content of the CSE is determined by the elemental carbon-to-oxygen ratio (C/O) of the AGB star itself, with  $C/O < 1$  leading to an oxygen-rich outflow and  $C/O > 1$  leading to a carbon-rich outflow (see, e.g., Habing & Olofsson 2003).

During the thermally pulsing AGB phase, low- and intermediate-mass stars develop strong mass loss and eject their envelope to become a short-lived (Siess et al. 2022). Stars are enshrouded by an optically thick dust shell, in which solids condense from the gas phase as tiny dust grains (Bowen 1988; Gail & Sedlmayr 1999). Dust is divided into O-rich dust and C-rich dust, pure thermal decomposition of olivine results in the formation of more silicon oxide dust (SiO), Mg, Fe, O (Gail & Sedlmayr 1999). C-rich dust mainly consists of amorphous carbon, and silicon carbide (SiC; Van de Sande et al. 2019). Since there are no condensation seeds in the gas simply outflowing from the star. In a series of physicochemical events, silicate dust grains eventually grow in the cooler outflows. The first step in the series of events leading to the growth of silicate dust grains in a cooling outflow must be the formation of seed particles. Because SiO is the most abundant of all gas-phase refractory elements that may

be involved in this process, there has been much discussion about whether it is the clusters formed from this substance that are the basis of all the processes? (Gail & Sedlmayr 1986; Ali & Castleman 2005; Nuth & Ferguson 2006; Paquette et al. 2011; Goumans & Bromley 2012)

Gail et al. (2013) show an upper limit to the stability of SiO based on new measurements of the vapor pressure of SiO molecules against solid SiO. SiO may be the first substance to nucleate out of a mixture of oxygen-rich elements (Nuth & Donn 1981). The dominant population ( $>0.9$ ) of presolar silicon carbide (SiC) are believed to have originated from low-mass AGB stars with close-to-solar metallicities (Liu & Stephan 2022). Some 90 years ago, Wildt (1933) considered the possibility that solid SiC grains might form in N-type stars. It is now recognized that SiC solids are a major dust species, second only to amorphous carbon particles, condensing in the cold atmospheres of mass-losing, carbon-rich AGB stars (Nanni et al. 2021; Chen et al. 2022). Spectroscopic observations have revealed the widespread presence of SiC dusts in carbon stars, with a prominent 11.3  $\mu\text{m}$  emission feature that characterizes the Si–C stretching of SiC solids (Speck et al. 1997; Mutschke et al. 1999). However, the exact mass fraction of condensate in the form of SiC in carbon stars is imprecise and depends on the stellar mass and metallicity (Nanni et al. 2021). Radiative transfer modeling of the observed infrared emission from carbon stars suggests that the mass ratio of SiC to amorphous carbon may be as high as 0.25 in the MW (Groenewegen et al. 1998), 0.43 in the LMC, and 0.11 in the

SMC (Groenewegen et al. 2009; Nanni et al. 2019). Theoretical dust yield calculations predict that the mass fraction of SiC produced in carbon stars out of the total dust is 0.25 of the total dust (i.e., silicon carbide plus amorphous carbon) for carbon stars with an initial mass of  $3 M_{\odot}$  in the vicinity of the solar metallicity (Nanni et al. 2013; Zhukovska & Henning 2013). Small molecules containing silicon and carbon are thought to be important components of interstellar particles. Some of them have been detected in the interstellar environments of late stars by rotational spectroscopy, such as SiC, SiC<sub>2</sub>, Si<sub>2</sub>C, c-SiC<sub>3</sub>, SiC<sub>4</sub>, while centrosymmetric species, such as C<sub>3</sub>, C<sub>4</sub>, C<sub>5</sub>, Si<sub>2</sub>C<sub>2</sub>, Si<sub>2</sub>C<sub>3</sub>, can only be detected by vibrational excursions (mainly in the infrared) (Witsch et al. 2017). Witsch et al. (2017) present laboratory data on the asymmetric stretching mode of Si<sub>2</sub>C at  $8.6 \mu\text{m}$ . They used a pulsed Nd:YAG laser to vaporize a solid Si target in a dilute methane sample exposed to helium buffer gas. Si<sub>2</sub>C was formed in the adiabatic expansion of a supersonic jet, and radiation from a quantum cascade laser was used to record rotationally resolved spectra.

Theoretical calculations (Gail & Sedlmayr 1986) based on the results of Nuth & Donn (1981) show that nucleation of SiO should not start until the temperature drops below  $\approx 600$  K, whereas observed condensation temperatures of periastron dust shells are typically in the range of 900 K and sometimes even higher.

The total ice number density and number of monolayers throughout the outflow depend on the temperature profile of the dust, with clear differences between the two amorphous carbonaceous grains and SiC dust (Van de Sande et al. 2019). The dust temperature profile of C-rich dust SiC is 350 K–500 K, according to the thesis of Van de Sande et al. (2019) can be obtained, where the C-rich dust mainly consists of large amounts of amorphous carbon and SiC. The dust temperature profile of O-rich dust is 550–800 K. The basic case of primary grain condensation can be best illustrated by stellar wind. Here, stellar wind refers to the basic situation of stellar outflow. For example, dust gas temperature and material dilution phenomena occur. There is a monotonic decrease in both gas temperature and matter density, which leads to a recolonization of the plasma and the appearance of diatoms, polyatoms, triatoms, tetraatoms, pentatoms, and hexatoms as the distance increases. As the distance increases, diatomic molecules, polyatomic molecules and finally composite molecules are formed. At certain distances, at temperatures well below 1500 K, certain atoms and molecules combine into stable clusters. The combination of atoms and molecules into stable clusters can lead to the formation of homogeneous or heterogeneous macroscopic samples by the addition of further similar or dissimilar substances (Sedlmayr 1994).

In recent years, many research groups have studied the dust and heavy elements (<sup>1</sup>H, <sup>12</sup>C, <sup>13</sup>C, <sup>14</sup>N, <sup>15</sup>N, and <sup>16</sup>O) yield of AGB stars (Ferrarotti & Gail 2006; Karakas & Lattanzio 2007; Ventura et al. 2020, 2021; Cinquegrana & Karakas 2022), and

in supernovae Wu et al. (2021). We estimated the abundance value of SiC in the solar system based on the spectrum, provided that the spectrum was corrected. Until now, only a few groups study the SiC and SiO dust condensation processes in AGB stellar winds, and infrared spectra of SiC dust. It has important research significance to the role of temperature on molecular dynamics, not only SiC, but also SiO, and the comparative analysis of its radiation spectrum. The study of the content and structure and spectra of SiC has a deeper role and impact.

The pressure magnitudes are  $[10^{-3}-10^{-6}]$  atm and  $[10^{-5}-10^{-6}]$  atm, respectively (Sedlmayr 1994; Van de Sande et al. 2019; Gail et al. 2020; Siess et al. 2022). Due to the very low pressure, down to  $10^{-6}$  atm, this effect will be ignored in this article. The topic of SiC and SiO dust condensation processes is especially important and fascinating. Because we can better understand the origin of SiC and SiO and the basic laws of stars, the evolution of ISM. It can be used as the James Webb Space Telescope (JWST) to observe the structure and study of dust. In Section 2, the physical parameters of the model used are summarized. Detailed results are discussed in Section 3. The conclusions are outlined in Section 4.

## 2. Models and Methods

We choose the Large-scale Atomic/Molecular Massively Parallel Simulator (LAMMPS) code to compute the SiC, SiO dust condensation process in the AGB stellar winds. LAMMPS is a classical molecular dynamics (MD) simulation code focusing on materials modeling. It was designed to efficiently run on parallel computers and to be easy to extend and modify. For simulation, it can be viscosity, diffusion coefficient, energy, radial distribution function, melting and solidification of spherical or ellipsoidal particles (<https://docs.lammps.org/Manual.html>) (Plimpton 1995; Denniston & Navid 2022). The model parameters are set as follows: SiC and SiO atoms were uniformly scattered with an initial spacing of  $2 \text{ \AA}$  in a simulation box sized  $20 \times 20 \times 20 \text{ \AA}^3$  with periodic boundaries. The box size of the particle heat bath is  $40 \times 40 \times 40$ . The timestep is 0.05 fs. The velocity of the atoms conforms to a Gaussian distribution. The system synthesis is NPT, because we want to consider the condensation of SiC, SiO dust at different temperatures and pressures. The temperature range for condensation of SiC dust in the AGB stellar wind is [300–500] k and [900–1100]k for SiO. The numbers of atoms of SiC and SiO dust are 100 and 121, respectively. Regarding the potential function, David et al. (2012) used LAMMPS to study the simulation of the initial oxidation process regarding O<sub>2</sub> and H<sub>2</sub>O molecules on the SiC surface. ReaxFF is able to naturally simulate the breaking and formation of interatomic bonds. This ReaxFF is also able to describe both Si–C–O and Si–O–H bond interactions. The ReaxFF force field, which is based on the principle of determining the bond levels according to the

distance between atoms, describes the interactions of the chemical system related to bonding according to the bond levels, and can smooth the transition of the system energies during bonding and bond breaking. Compared with the conventional force field, the ReaxFF force field provides a better description of the polarization because the atomic charges are dynamically optimized using the electronegativity balance method at each time step in the simulation. Compared with quantum mechanics, the ReaxFF molecular simulation is more suitable for complex systems because the reaction paths can be determined entirely by system driving (Du & Wang 2018). In most cases, LAMMPS numerically integrates the Newtonian equations of motion for particles such as atoms, molecules or macroscopic particles. At the beginning of the program, the expressions for the resolved force and potential energy in the discrete coordinate positions are computed and stored in an array. The simulation process uses the sample strip interpolation is used in the simulation to obtain accurate force and potential energy values. Mean square displacement (MSD): the square of the average distance ( $r$ ) is traveled by the particles at time  $t$  interval.

$$\langle r^2(t) \rangle = \frac{1}{N} \sum_{i=1}^N \Delta r_i^2(t). \quad (1)$$

Here,  $N$  denotes the number of atoms. Diffusion coefficient:  $\langle r^2(t) \rangle = 2dD$ , where  $d$  is the dimension. Velocity autocorrelation function (VACF)  $\langle v(t)v(0) \rangle$ :

$$D = \int_0^{t_\infty} \langle v(t)v(0) \rangle dt, \quad (2)$$

Infrared radiation spectra obtained by Gaussian 16 calculation. A uniform broadening (Lorentzian line shape) imposed by Gaussian software to simulate real spectral lines. In general, electronic spectra (UV-Vis, ECD) are broadened with Gaussian functions, and vibrational spectra (IR, Raman, VCD) are broadened with Lorentzian functions, which decay more slowly than Gaussian functions. According to the uniform bandwidth—Lorentzian line equation:

$$I(\omega) = \frac{I_{\max} \left( \frac{1}{4\tau^2} \right)}{(\omega - \omega_0^2) + \left( \frac{1}{4\tau^2} \right)}. \quad (3)$$

The lifetime bandwidth over the wavenumber is  $\nu = 5.3/\tau(\text{cm}^{-1} \text{ps}^{-1})$ . For a quantum state with a lifetime of  $\tau$ . When we take the frequency mean interval  $\omega - \omega_0^2$  as 10. In Equation (3), we take half the size of radiation intensity  $I(\omega)$ , like  $I(\omega)/2$ . We can obtain Equation (4).  $I_{\max}$  represents the maximum radiation intensity. About  $I(\omega)$ , the bandwidth  $\nu$  range obtained after taking the maximum and minimum values of the radiation intensity is 0.1–0.5 nm.

$$\tau = \sqrt{\frac{I_{\max}}{2I(\omega)(\omega - \omega_0^2)} - \frac{1}{4(\omega - \omega_0^2)}}. \quad (4)$$

Infrared spectral (IR) calculations were performed on the final structure of LAMMPS after applying the temperature. IR spectroscopy originates from vibrational jumps and consists of measuring the absorption of matter exposed to light at a range of IR frequencies. The total amount of energy absorbed is called the intensity, which is plotted as the height of the peak at that frequency. The spectrum thus obtained is a unique identifier of a molecule's constituent atoms and bonding (i.e., its structure). We applied the density functional theory (DFT). Regarding the generalization we chose B3LYP with the basis group 6–21g. The B3LYP function is a popular and well-regarded function that is primarily calculated for metal oxides and other inorganic compounds. The researchers calculated the asymmetric model also using the B3LYP function (Lee et al. 1988). The first step calculation is to obtain the self-consistent energy, optimized atomic configuration and spin density. Required convergence on the root mean square density matrix was less than  $10^{-8}$ . A single scale factor of 0.965 was used to compare the DFT harmonic wavelength NDFT ( $\text{cm}^{-1}$ ) with the experimental data (Ota 2015). Corrected wavenumber  $N$  is obtained simply by  $N (\text{cm}^{-1}) = \text{NDFT} (\text{cm}^{-1}) \times 0.965$ . Wavelength  $\lambda$  is obtained by  $\lambda (\mu\text{m}) = 10,000/N(\text{cm}^{-1})$  (Ota 2019).

### 3. Results

Our results show that 100 atoms of SiC, SiO are stabilized by molecular dynamics stabilization calculations to obtain the final stabilized structure. Among them, the 77SiC, 70Si<sub>3</sub>C<sub>3</sub>, and 121Si<sub>3</sub>C<sub>3</sub> models have characteristic peaks of infrared spectra responding at 5, 11.3, 15, 19, and 37  $\mu\text{m}$ , which are represented by curves with different colors respectively.

#### 3.1. SiC and SiO Molecular Dynamics and Spectral Calculations for SiC

The classical process of dust formation is divided into two steps. First, critical clusters are formed that act as seeds of condensation, and then the dust grains are grown to macroscopic size by the addition of small entities called monomers. Second, the dust grains are grown to macroscopic size by adding small monomers entities (Siess et al. 2022). In Figure 1, the initial structure of the 121Si<sub>3</sub>C<sub>3</sub> models comes from the work of Wu et al. (2022). Si<sub>3</sub>C<sub>3</sub> was chosen because it is the smallest cluster with a three-dimensional structure (see Gobrecht et al. (2017)), so we could study the spectra of the low-end clusters. Our reasons for choosing the three molecular structures 77SiC, 70Si<sub>3</sub>C<sub>3</sub> and 121Si<sub>3</sub>C<sub>3</sub> as representatives for the IR spectral calculations include the following two main points. The first is that few researchers have calculated the IR spectra of the above three molecular structures. The second reason is that the above three molecules are easy to calculate the non-spherical spectra and easy to replicate the established

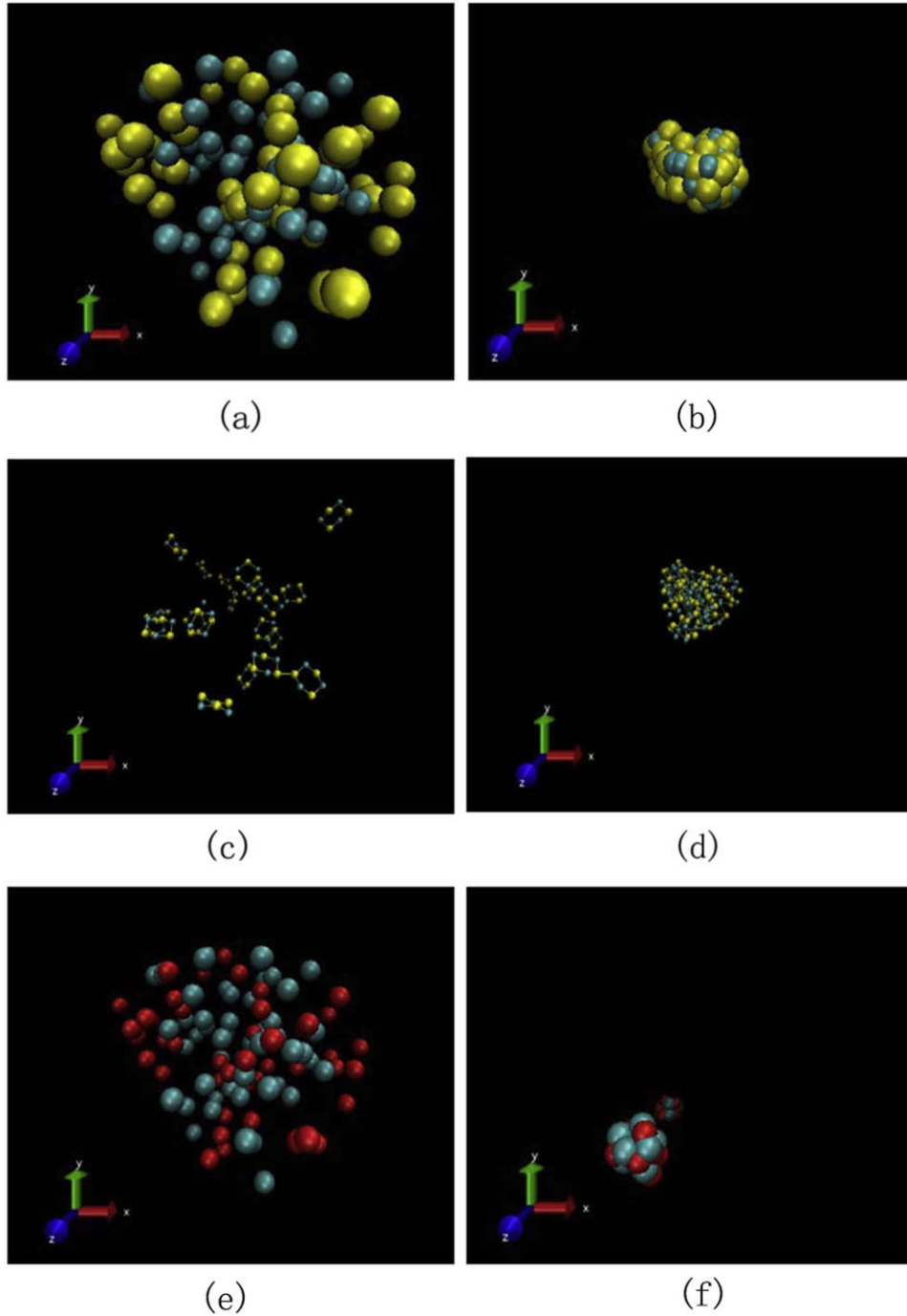


**Figure 1.** Subfigure (a) shows the initial distribution of 100SiC molecules in a box size of  $40 \times 40 \times 40$ , and subfigure (b) shows the final coalescence of 77SiC molecules into nuclei in the box. Subfigure (c) shows the initial distribution of 121Si<sub>3</sub>C<sub>3</sub> molecules in a box size of  $40 \times 40 \times 40$ , and subfigure (d) shows the final coalescence of 121Si<sub>3</sub>C<sub>3</sub> molecules into multiple small dust nuclei in the box. Here the number 121 indicates the total number of atoms of the structure. Similarly, subfigure (e) shows the initial distribution of 100SiO molecules in a box size of  $40 \times 40 \times 40$ , and subfigure (f) shows the final coalescence of 100SiO molecules into multiple small dust nuclei in the box. In the figure, the yellow atoms are C, the red atoms are O, and the blue atoms are Si.

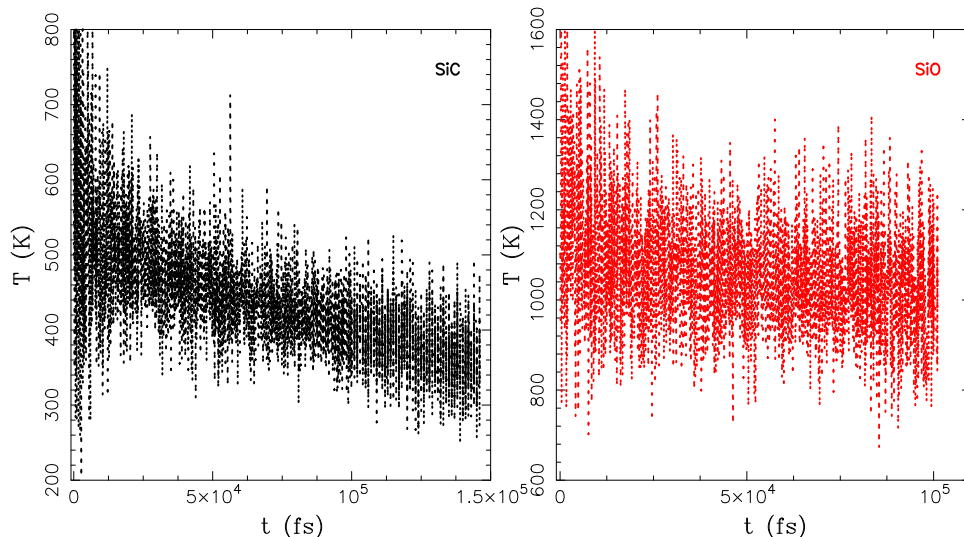


**Figure 2.** The left and right graphs show the trend of temperature with time for SiC, SiO molecules. The black line represents SiC molecules, and the red line represents SiO molecules.

model, which is convenient for us to calculate other physical properties at a later stage. So we chose the above three molecular models as the main model calculation. For LAMMPS, the basic principle of molecular dynamics is the use of Newtonian mechanical equations to describe the positions, velocities, and interatomic interactions of atoms, and by solving these equations, it is possible to simulate the kinetic behavior of molecules and to compute the kinetic behavior of large-size systems. We can see that the atoms coalesce into small SiC and SiO clusters due to interactions. It mainly consists of the attractive and repulsive forces between molecules. In the gaseous state, the smaller the intermolecular distance, the weaker the intermolecular interaction, and vice versa, the stronger the interaction force. When the molecules are at high temperature or high pressure, the intermolecular spacing gradually shrinks, which will produce a large amount of absorbed or released heat, the gravitational force is formed by the charge interaction of molecules, when the distance between molecules is not changing, and finally leads to changes in morphology, the formation of a solid. In Figure 2, the temperature is calculated by dividing the kinetic energy by a certain number of degrees of freedom (and the Boltzmann constant). Since kinetic energy is a function of the particle velocity, it is often necessary to distinguish between the advective velocity of a particle (due to the aggregation motion of some particles) and its thermal velocity. The sum of the two is the total velocity of the particle, but the latter is usually the temperature that we want to calculate. Let us perform a constant NPT system to update the position, velocity, and angular velocity of a finite-size  $x$ -spherical particle for each time step (refer to <https://docs.lammps.org>). The initial

temperature of the SiC molecule drops from 500 to 300 K, where the pressure is so small that we ignore its effect (refer to the work of Hanine et al. (2020)), and the highest temperature in the figure can even be as high as 800 K, due to the intermolecular forces being so strong that they cause the temperature to rise. Similarly, the initial temperature of the SiO molecule decreases from 1100 to 900 K, with a maximum temperature of 1600 K. In Figure 3, the total energy of the two molecules is demonstrated to reach a stabilization value, showing the stabilization of the final structure and the molecular dynamics reaching an equilibrium state. Both models are down to equilibrium trend. For example, the final total energy of the SiC dust cluster is as low as  $-1.2 \times 10^4 \text{ kcal mole}^{-1}$ , the SiC cluster mass size  $3.31 \times 10^{-24} \text{ kg}$ . SiO cluster mass size ranges from  $3.65 \times 10^{-25}$  to  $7.3 \times 10^{-25} \text{ kg}$ . Energy includes kinetic energy  $E1 = 0.5mv^2$ , potential energy  $E2 = mgh$ , where “ $m$ ” is the mass of the atom and “ $v$ ” is the velocity value. “ $h$ ” is the distance traveled by the atom. Rotational energy  $E3 = 0.5I\omega^2$ . Here, “ $E$ ” represents the rotational kinetic energy of the atom, “ $I$ ” is the rotational moment of inertia of the atom, “ $\omega$ ” is the angular velocity of the atom.

In Figure 4, the horizontal coordinate indicates the wavelength and the vertical coordinate indicates the magnitude of the radiation intensity.  $^{77}\text{SiC}$  model has peaks at wavelengths of 6, 8.6, 10, 15, 20, 31, 33  $\mu\text{m}$ , respectively. In particular, there is a strong characteristic peak at 15  $\mu\text{m}$ , which we find to be due to a large amount of Si–C bond stretching. As shown in Figure 5 right, the Si–C, Si–Si bond length scaling of the structure on the right side of the blue solid line is more significant than that on the left side of the scale.  $^{121}\text{Si}_3\text{C}_3$

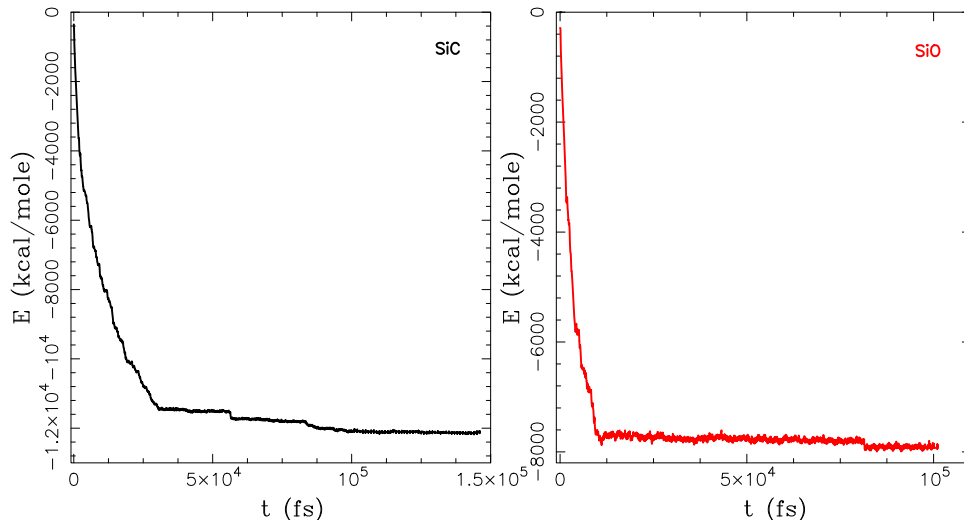


**Figure 3.** The evolution curve of the total energy ( $E$ ) of SiC, and SiO molecules over time is shown, with a decreasing to smooth trend in the total energy.

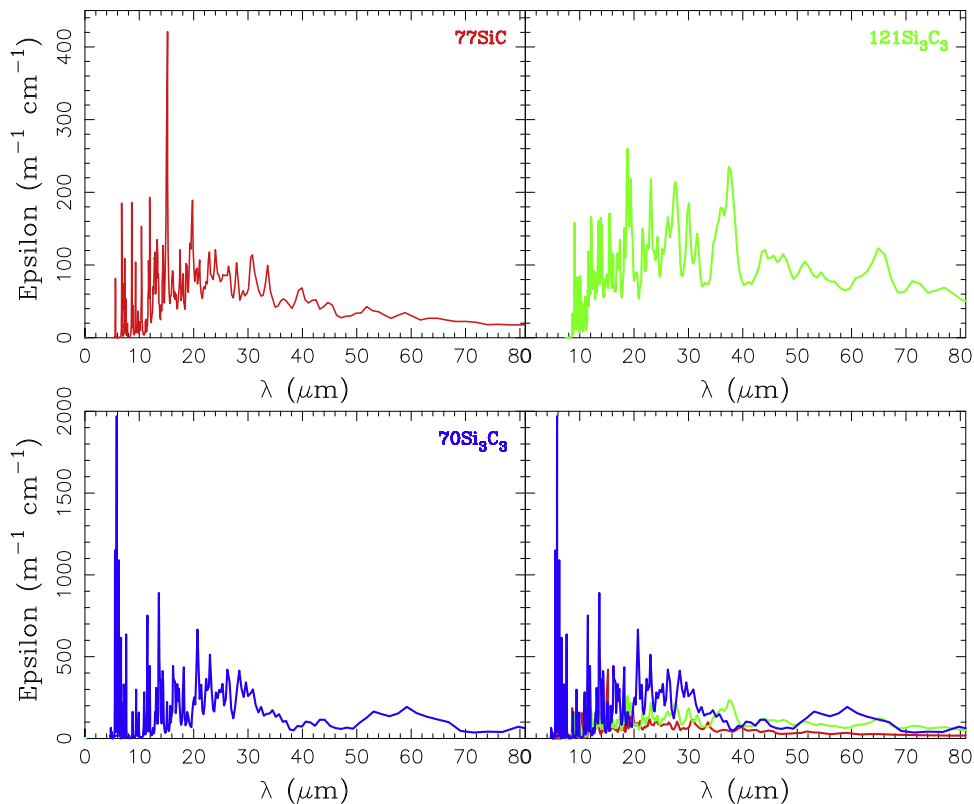


**Figure 4.** The infrared spectra of model 77SiC are represented by the red curve, and the remaining models 121Si<sub>3</sub>C<sub>3</sub> and 70Si<sub>3</sub>C<sub>3</sub> are represented by green and dark blue, respectively. The figure in the lower right corner shows a comparison of the infrared spectra of the three models.

model has peaks at wavelengths of 8.6, 12, 16, 19, 23, 27, 29, 37, and 66  $\mu\text{m}$ , respectively. In particular, there are two strong characteristic peaks at 19, 37  $\mu\text{m}$ , which we consider to be due to the large amount of Si-C, Si-Si bond stretching. As shown

in Figure 5 left, the Si-C, C=C bond length scaling of the structure on the right side of the blue solid line is more significant than that on the left side of the scale. The 70Si<sub>3</sub>C<sub>3</sub> model has peaks at wavelengths of 5, 11.3, 14, 17, 18, 21, 29,

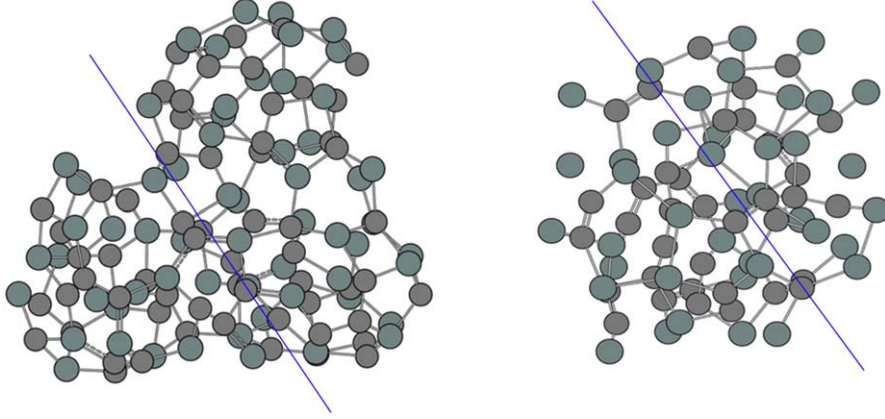


**Figure 5.** The picture on the left shows model  $121\text{Si}_3\text{C}_3$  and the picture on the right shows model  $77\text{SiC}$ , where the gray atoms are represented as C atoms and the dark green atoms are Si atoms.

53, 60  $\mu\text{m}$ , respectively. In particular, there are two strong characteristic peaks at 5, 11.3  $\mu\text{m}$ , which we consider to be due to a large amount of Si–C bond stretching. Among the three models, the  $70\text{Si}_3\text{C}_3$  model has the highest radiation intensity.  $121\text{Si}_3\text{C}_3$  and  $77\text{SiC}$  models have decreasing radiation intensity in that order. Regarding the radiative signature of SiC at 11.3  $\mu\text{m}$  (Speck et al. 1997; Mutschke et al. 1999), only model  $70\text{Si}_3\text{C}_3$  of our model has a significantly radiative signature, and the remaining two models are apparently not significant, and we consider that this is due to the weaker Si–C bond scaling and the stronger Si–Si, C=C bond scaling. Witsch et al. (2017) presented laboratory results for the asymmetric stretching mode of  $\text{Si}_2\text{C}$  at 8.6  $\mu\text{m}$ . Here we obtain this peaks for both  $77\text{SiC}$  and  $121\text{Si}_3\text{C}_3$  models. This result provided theoretical support for later observations of dust in the ISM. We consider still the peak due to Si–C bond stretching. This calculation is of great significance for the future budget of the output of stellar dust, galaxy dust, and the influence of dust radiation spectra on observations. For example, it can serve as a reference for dust observations by the JWST, the Large Sky Area Multi–Object Fiber Spectroscopy Telescope (LAMOST), and the upcoming China Space Station Optical Survey Telescope (CSST).

We estimated the abundance value of SiC in the solar system based on the spectrum and calculated it as follows: the infrared emissivity per unit mass of SiC molecules is

$$(j_\lambda/m) = \frac{C_{\text{abs}}(a, \lambda)}{m} 4\Pi B_\lambda(T). \quad (5)$$

The mass absorption coefficient is

$$\frac{C_{\text{abs}}}{\frac{4}{3}\Pi a^3 \rho} = \frac{3C_{\text{abs}}}{4\Pi a^3 \rho}. \quad (6)$$

The absorption cross-section is

$$C_{\text{abs}} = \Pi a^2 Q_{\text{abs}}(\lambda). \quad (7)$$

The above formula can obtain:

$$(j_\lambda/m) = \frac{3Q_{\text{abs}}(\lambda)}{a\rho} \Pi B_\lambda(T). \quad (8)$$

If SiC has a radiation flux of  $F_\lambda$  at 11.3  $\mu\text{m}$ , the distance between a star and Earth is  $d$ .

$$F_\lambda = \frac{M_{\text{SiC}}(j_\lambda/m)}{4\Pi d^2}. \quad (9)$$

According to formulas (8) and (9), the following equation can be obtained:

$$M_{\text{SiC}} = F_\lambda d^2 \frac{4a\rho}{3Q_{\text{abs}}(\lambda)B_\lambda(T)}. \quad (10)$$

Here, we have made corrections to  $F_\lambda$  by multiplying it by  $10^{-30}$  to match the observed spectrum. Using the distance  $d$  between the Sun and the Earth ( $d = 1.47 \times 10^{11}$  m). The frequency is  $2.75 \times 10^{12}$  Hz. The absorption efficiency factor  $Q_{\text{abs}}$  is 0.7, dust density  $\rho$  is  $3.22 \text{ g cm}^{-3}$ , dust radius  $a$  is  $1.17 \times 10^{-9}$  m, and the Planck function  $B_\lambda(T)$  is  $2.28 \times 10^{-15}$ . By substituting the above parameters into Equation (10), the abundance value of SiC ( $M_{\text{SiC}}$ ) can be obtained.  $M_{\text{SiC}}$  is  $4.75 \times 10^{-5}$ , which happens to be within the corresponding range of  $10^{-6}$ – $10^{-3}$  for Ferrarotti & Gail (2006) job.

## 4. Conclusions

Through MD simulations, we modeled the process of atoms coalescing into small clusters of SiC and SiO in AGB stellar winds. It was observed that the initial temperature of SiC molecules decreased from 500 to 300 K, while that of SiO molecules decreased from 1100 to 900 K. SiC molecules condensed entirely into a single cluster, whereas SiO molecules condensed into multiple small clusters within an evolution time of up to  $10^5$  fs.

Furthermore, we analyzed the infrared spectrum of SiC nanoparticles. It was found that the  $77\text{SiC}$ ,  $70\text{Si}_3\text{C}_3$ , and  $121\text{Si}_3\text{C}_3$  molecules exhibited characteristic peaks at 5, 8.6, 11.3, 15, 19, and  $37\ \mu\text{m}$ . Specifically, the  $77\text{SiC}$  molecule exhibited peaks at 8.6 and  $15\ \mu\text{m}$ , the  $70\text{Si}_3\text{C}_3$  molecule exhibited peaks at 5 and  $11.3\ \mu\text{m}$ , and the  $121\text{Si}_3\text{C}_3$  molecule exhibited peaks at 8.6, 19, and  $37\ \mu\text{m}$ . Many of these peaks corresponded to the Si–C bond stretching mode.

### Acknowledgments

We would like to thank Professor Aigen Li of the University of Missouri, Professor Zhao Wang from Guangxi University, and Dr. Dandan Wei of the Heidelberg University for their help and discussions. Moreover, we are grateful for resources from the High-Performance Computing Center of Central South University. This work received such generous support of the Independent Innovation Project for Postgraduates of Central South University No. 160171008. This work is supported by the National Natural Science Foundation of China, and projects Nos. 11803026, U2031204.

### References

- Ali, A., & Castleman, A. W. 2005, in *Astrochemistry: Recent Successes and Current Challenges*, ed. D. C. Lis, G. A. Blake, & E. Herbst, Vol. 231 (Cambridge: Cambridge Univ. Press), 107, *Astrochemistry: Recent Successes and Current Challenges*
- Bowen, G. H. 1988, *ApJ*, 329, 299
- Chen, T., Xiao, C. Y., Li, A., & Zhou, C. T. 2022, *MNRAS*, 509, 5231
- Cinquegrana, G. C., & Karakas, A. I. 2022, *MNRAS*, 510, 1557
- David, Z. B., Sengupta, D., & Foroutan, H. 2012, *JPhCh*, 116, 16111
- Denniston, C. A., & Navid, M. G. 2022, *CoPhC*, 275, 1
- Du, L., & Wang, W. J. 2018, *High Voltage*, 2, 151
- Ferrarotti, A. S., & Gail, H. P. 2006, *A&A*, 447, 553
- Gail, H. P., & Sedlmayr, E. 1986, *A&A*, 166, 225
- Gail, H. P., & Sedlmayr, E. 1999, *A&A*, 347, 594
- Gail, H.-P., Tamanai, A., Pucci, A., & Dohmen, R. 2020, *A&A*, 644, A139
- Gail, H. P., Wetzel, S., Pucci, A., & Tamanai, A. 2013, *A&A*, 555, A119
- Gobrecht, D., Cristallo, S., Piersanti, L., & Bromley, S. T. 2017, *ApJ*, 840, 117
- Goumans, T. P. M., & Bromley, S. T. 2012, *MNRAS*, 420, 3344
- Groenewegen, M. A. T., Sloan, G. C., Soszyński, I., & Petersen, E. A. 2009, *A&A*, 506, 1277
- Groenewegen, M. A. T., Whitelock, P. A., Smith, C. H., & Kerschbaum, F. 1998, *MNRAS*, 293, 18
- Habing, H. J., & Olofsson, H. 2003, *A&A*, 62, 78
- Hanine, M., Meng, Z., Lu, S., et al. 2020, *ApJ*, 900, 188
- Karakas, A., & Lattanzio, J. C. 2007, *PASA*, 24, 103
- Lee, C., Yang, W., & Parr, R. G. 1988, *PhRvB*, 37, 785
- Liu, N., & Stephan, T. 2022, *LPI Contributions*, 2695, 151
- Mutschke, H., Andersen, A. C., Clément, D., Henning, T., & Peiter, G. 1999, *A&A*, 345, 187
- Nanni, A., Bressan, A., Marigo, P., & Girardi, L. 2013, *MNRAS*, 434, 2390
- Nanni, A., Cristallo, S., van Loon, J. T., & Groenewegen, M. A. T. 2021, *Univ*, 7, 233
- Nanni, A., Groenewegen, M. A. T., Aringer, B., et al. 2019, *MNRAS*, 487, 502
- Nuth, J. A., & Donn, B. 1981, *ApJ*, 247, 925
- Nuth, J. A. I., & Ferguson, F. T. 2006, *ApJ*, 649, 1178
- Ota, N. 2015, arXiv:1502.01766
- Ota, N. 2019, arXiv:1904.10140
- Paquette, J. A., Ferguson, F. T., & Nuth, J. A. I. 2011, *ApJ*, 732, 62
- Plimpton, S. 1995, *JCoPh*, 171, 1
- Sedlmayr, E. 1994, in *IAU Coll. 146: Molecules in the Stellar Environment*, Vol. 428, ed. U. G. Jorgensen (Berlin: Springer), 163
- Siess, L., Homan, W., Toupin, S., & Price, D. J. 2022, *A&A*, 667, A75
- Speck, A. K., Barlow, M. J., & Skinner, C. J. 1997, *MNRAS*, 288, 431
- Van de Sande, M., Walsh, C., Mangan, T. P., & Decin, L. 2019, *MNRAS*, 490, 2023
- Ventura, P., Dell’Aglia, F., Lugaro, M., et al. 2020, *A&A*, 641, A103
- Ventura, P., Dell’Aglia, F., Romano, D., et al. 2021, *A&A*, 655, A6
- Wildt, R. 1933, *ZA*, 6, 345
- Witsch, D., Lutter, V., Fuchs, G. W., Gauss, J., & Giesen, T. 2017, in *72nd Int. Symp. Molecular Spectroscopy*, WA07 WA07
- Wu, R.-Q., Long, M.-Q., Zhang, X.-J., et al. 2022, *RAA*, 22, 035014
- Wu, R.-Q., Zhu, C.-H., Lü, G.-L., Wang, Z.-J., & Liu, H.-L. 2021, *RAA*, 21, 129
- Zhukovska, S., & Henning, T. 2013, *A&A*, 555, A99